Proceedings of the ASME 2016 Power & Energy Conference & Exhibition
PowerEnergy2016
June 26-30, 2016, Charlotte, North Carolina, USA

PowerEnergy2016-59160

DESIGN OF A MODULAR SOLID-BASED THERMAL ENERGY STORAGE FOR A HYBRID COMPRESSED AIR ENERGY STORAGE SYSTEM

Reza Baghaei Lakeh, Ph.D.
California State Polytechnic University
Pomona, California, USA

Ian C. Villazana*
California State Polytechnic University
Pomona, California, USA

Sammy Houssainy
University of California Los Angeles
Los Angeles, California, USA

Kevin R. Anderson, Ph.D.
California State Polytechnic University
Pomona, California, USA

H. Pirouz Kavehpour, Ph.D.
University of California Los Angeles
Los Angeles, California, USA

ABSTRACT

The share of renewable energy sources in the power grid is showing an increasing trend world-wide. Most of the renewable energy sources are intermittent and have generation peaks that do not correlate with peak demand. The stability of the power grid is highly dependent on the balance between power generation and demand. Compressed Air Energy Storage (CAES) systems have been utilized to receive and store the electrical energy from the grid during off-peak hours and play the role of an auxiliary power plant during peak hours. Using Thermal Energy Storage (TES) systems with CAES technology is shown to increase the efficiency and reduce the cost of generated power. In this study, a modular solid-based TES system is designed to store thermal energy converted from grid power. The TES system stores the energy in the form of internal energy of the storage medium up to 900 K. A three-dimensional computational study using commercial software (ANSYS Fluent) was completed to test the performance of the modular design of the TES. It was shown that solid-state TES, using conventional concrete and an array of circular fins with embedded heaters, can be used for storing heat for a high temperature hybrid CAES (HTH-CAES) system.

INTRODUCTION

Energy storage has proven to be a viable option for generating power during peak hours, particularly in an electric power industry that is rapidly changing. Fluctuations in demand of electricity can be attributed to changes in consumer behavior, emerging technologies and regulations [1]. When the demand for electricity is the highest, consumers are imposed a high demand charge ($/kW) and investor-owned utilities (IOUs) also incur high costs to provide that electricity to consumers. Renewable energy technologies, such as solar and wind, produce electricity in intermittent cycles and the availability of electricity during peak hours can be often unpredictable. This results in a mismatch between the supply and demand of energy. The solution to producing a more predictable and manageable form of energy lies in energy storage.

Different technologies have been utilized for utility-scale energy storage, including pumped hydro-power, low friction flywheels, thermal and thermochemical energy storage, grid-scale batteries. Compressed air energy storage (CAES) works based on compressing the air during off-peak hours and storing the pressurized air for future use. During the discharge cycle, the pressurized air is utilized to run a turbine to generate power. Conventional diabatic CAES systems has been commercialized. Currently, two operational power plants in Alabama (110 MW built in 1991) and Germany (290 MW plant built in 1978) are using this technology to store energy [2-3]. The efficiency of the conventional CAES systems are impacted by losing the heat of compression. Advanced Adiabatic CAES (AA-CAES) systems are proposed to capture the heat of compression in the charge cycle and store the heat in a TES system. The stored thermal energy is used to heat the air prior to expansion. The recovery of the compression heat using AA-CAES eliminates the need for

*villazana.ian@gmail.com

fossil fuel consumption in conventional CAES power plants. Although AA-CAES systems are expected to increase the round-trip efficiency of energy storage, a fully operational AA-CAES system is yet to be demonstrated in utility scale [4].

In a recent study, a High Temperature Hybrid Compressed Air Energy Storage (HTH-CAES) is considered. In order to reduce the heat of compression, a high-temperature TES system is directly charged by the power grid through joule heating. The stored heat in the TES is utilized to provide the compressed air with the required enthalpy to run a power block. The concept of HTH-CAES, along with thermodynamic model of the system, is discussed in further details in reference [5]. The design of a solid-state TES system used for the HTH-CAES system is explored in this study. Although different TES options are available for the proposed system [6-9], a concrete TES system was considered due to its low investment cost. The chief advantages of a concrete TES system are the low capital cost per unit of electricity ($/kWh), maintenance cost, high specific heat, and solid mechanical properties [10]. The greatest disadvantage in a concrete TES system lies in the thermal properties of concrete. Although the material properties of concrete lend itself for systems of these types, the thermal conductivity of concrete is relatively low, impeding heat transfer. It will be shown later in this paper that this can be overcome with a proper TES design that includes the use of finned tubes to promote heat transfer.

Figure 1 shows a schematic of the HTH-CAES concept. The heat is generated by electrical heaters that are placed within the TES module to eliminate the need for heat transfer fluids. The compressed air that is stored in a high pressure tank is used during the discharge cycle to extract the heat from the TES modules. The released thermal energy increases the enthalpy of the air. The high temperature, high pressure air is then introduced to a power generation unit. The TES system is designed in the form of cascaded modules. In order to enhance the performance of the system, an array of stainless steel fins is utilized to enhance the heat transfer during charge and discharge cycles. The solid-based and modular thermal storage unit is designed to provide 6 hours of air temperature above 850 K at a flow rate of 1 kg/s. These input conditions are required to ensure the functionality of the expander, as shown in Fig. 1.

THERMAL MODEL DESCRIPTION

The TES system analyzed in this paper is a vital piece to a large scale HTH-CAES system design. The overall HTH-CAES system consists of a compressor, a heat exchanger (HX) to extract heat from the compressed air, a compressed air tank, a low temperature thermal energy storage (LTES) system, an LTES HX between the compressed air tank and LTES system, a high temperature thermal energy storage (HTES) system, a microturbine, a steam cycle system, and a HX for transfer of heat between the microturbine exhaust and the steam cycle system. Figure 1 shows the overall HTH-CAES system. The concrete TES system presented in this paper is the HTES system feeding the microturbine high temperature air. The HTES system is charged thermally by converting grid power to thermal energy through joule heating.

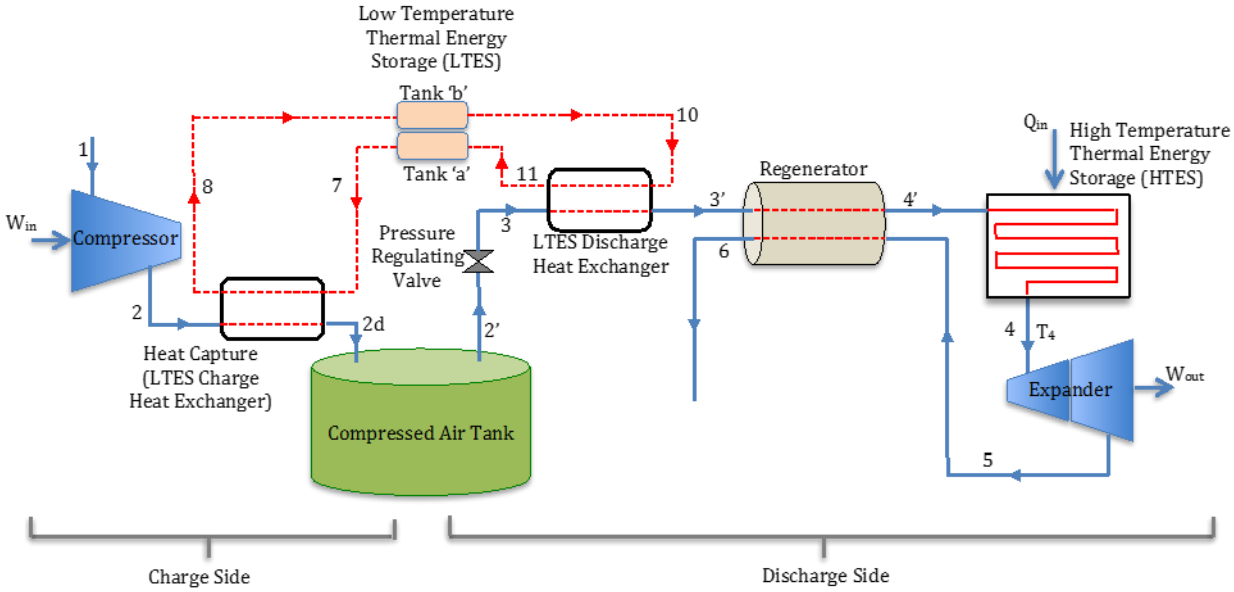

Figure 1 – High Temperature Hybrid Compressed Air Energy Storage (HTH-CAES) System

During the discharge cycle, the air leaves the storage tank and receives the heat of compression stored in Low Temperature Thermal Energy Storage (LTES) and enters the High Temperature Thermal Energy Storage (HTES). The HTES is designed to provide over 6 hours of air temperature above 850 K. The exhaust air temperature exiting the expander is fed to a regenerator to increase the efficiency of the system.

One of the most important objectives of the computations of this study was to develop a cost-effective design that would not only provide the best thermal performance, but also the most adequate exit air temperature profile to be fed to the expander. For simplicity, an axisymmetric model containing only 1/4th of the concrete TES module was modeled and analyzed using ANSYS Fluent 16.1. This was done to reduce the total number of finite volume cells and reduce the computation time. The simulations were completed on a standard 8-core, 16-megabyte memory desktop computer.

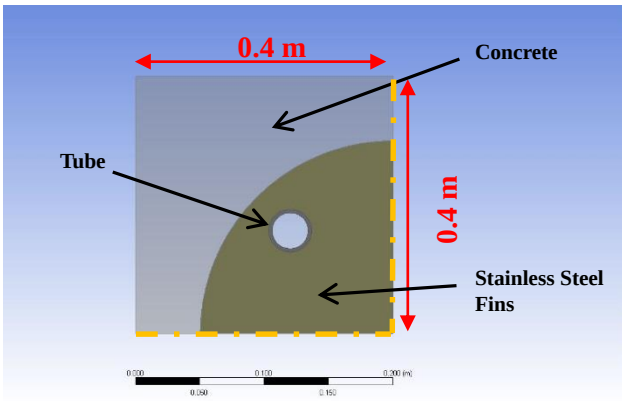

Figure 2 – Front View of Concrete TES System

As illustrated in Figs 2-3, a complete TES module is comprised of the following major components: a rectangular concrete body, circular stainless steel fins, and four thin-walled stainless steel tubes. The working fluid selected for this system was air. A single and complete TES module fits within an envelope of 8 m by 0.4 m by 0.4 m. The four thin-walled tubes, each 8 m in length, run longitudinally across the rectangular body, which is also 8 m in length. In a complete TES module, the thin-walled tubes are spaced 0.16 m apart and are laid out in a square configuration. 317 circular fins were placed over the thin-walled tubes to increase surface area and improve heat transfer. In practice, each circular fin would be welded on to each of the four thin-walled tubes to create finned tubes. The fins are placed 0.0125 m apart to further enhance heat transfer to and from the concrete body during charge and discharge cycles. The circular fins are 0.30 m in diameter and extend up to 0.05 m apart from the concrete body's inner walls. Because thermal energy will be converted from the power grid through Joule heating, volumetric heat generation (W/m^3) is assumed to develop uniformly in all circular fins. In practice, this would simulate electric resistance strips mounted across all fins.

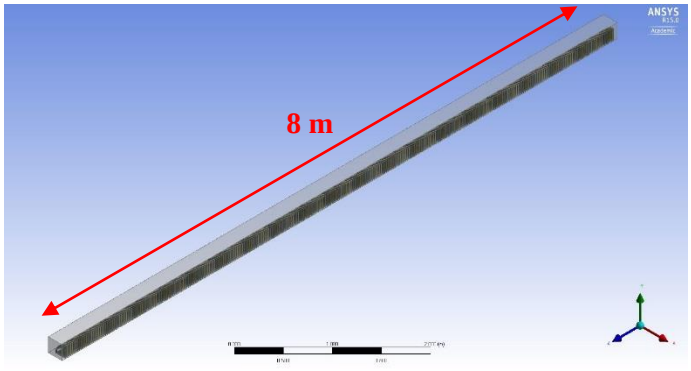

Figure 3 – Isometric View of Concrete TES System

The overall system is designed in the form of cascaded TES modules in series, as shown in Fig. 4. However, four thin-walled tubes will run in parallel in each TES module. This is done in an effort to receive the thermal energy stored in the concrete and fins. In practice, the air entering each TES module would be distributed to each tube by means of a common header.

Figure 4 – Schematic of Cascaded TES Modules

The governing equations of the problem are the continuity, momentum, and energy equation.

$$\frac{\partial \rho}{\partial t} + \frac{\partial (\rho v_j)}{\partial x_j} = 0 \tag{1}$$

$$\frac{\partial (\rho v_i)}{\partial t} + \frac{\partial (\rho v_i v_j)}{\partial x_j} = -\frac{\partial P}{\partial x_i} + \frac{\partial}{\partial x_j}\left[(\mu + \mu_t)\left(\frac{\partial v_i}{\partial x_j} + \frac{\partial v_j}{\partial x_i}\right)\right] + \rho g_i \tag{2}$$

$$\frac{\partial (\rho h)}{\partial t} + \frac{\partial (\rho v_j h)}{\partial x_j} = \frac{\partial}{\partial x_j}\left[(\lambda + \lambda_t)\frac{\partial T}{\partial x_j}\right] + \dot{G} \tag{3}$$

The variables v_i, P, and T represent the mean values in turbulent computations. A standard k-ε model [11-12] is utilized to model Reynolds stresses in turbulent computations. The last term on the right hand side of Eq. (3) represent the heat generation by Joule heating in the electrical heaters that are embedded in the annular fins. During the charge cycle, heat generation, i.e., $\dot{G}$ is assumed to be zero in all parts of the solution domain except for the fins. During discharging, the heat generation is switched off for all parts. The transport of turbulence kinetic energy and dissipation are governed by Eqs. (4-5).

$$\frac{\partial(\rho k)}{\partial t} + \frac{\partial\left(\rho k v_j\right)}{\partial x_j} = \frac{\partial}{\partial x_j}\left[\left(\mu + \frac{\mu_t}{\sigma_k}\right)\frac{\partial k}{\partial x_j}\right] - \rho\varepsilon + G_k + G_b \quad (4)$$

$$\frac{\partial(\rho \varepsilon)}{\partial t} + \frac{\partial\left(\rho \varepsilon v_j\right)}{\partial x_j} = \frac{\partial}{\partial x_j}\left[\left(\mu + \frac{\mu_t}{\sigma_\varepsilon}\right)\frac{\partial \varepsilon}{\partial x_j}\right] - C_{2\varepsilon}\rho\frac{\varepsilon^2}{k} + C_{1\varepsilon}\frac{\varepsilon}{k}(G_k + C_{3\varepsilon}G_b) \quad (5)$$

The generation of turbulence kinetic energy due to shear, G_k, and buoyancy, G_b, are obtained from Eqs. (6-7).

$$G_k = \mu_t S^2 \ , \quad S_{ij} = \frac{1}{2}\left(\frac{\partial v_i}{\partial x_j} + \frac{\partial v_j}{\partial x_i}\right) \quad (6)$$

$$G_b = \beta g_i \frac{\mu_t}{\sigma_t}\frac{\partial T}{\partial x_i} \quad (7)$$

Symmetric boundary conditions were assigned to the bottom and side face of the concrete body (facing the x-axis and y-axis in Fig. 2). The concrete's exterior walls were set to be insulated. The tube inlet was designated as a mass flow inlet type, where inlet mass flow rate and inlet temperature were specified. The tube outlet was designated as a pressure outlet. Note that a constant temperature is specified at the inlet of the 1st TES module only. However, because the overall system is designed in the form of cascaded TES modules, a transient inlet boundary condition is necessary after the 1st TES module. In defining the inlet temperature of TES Module 2, a profile is created using the recorded exit air temperature of the preceding TES module.

The governing equations were discretized using a finite-volume method and an implicit and second-order upwind scheme was used to interpolate the convective terms in momentum, energy, turbulence kinetic energy, and turbulence dissipation equations. A grid-refinement study was conducted to ensure independency of the results to the number of grid points. The commercial software ANSYS Fluent 16.1 was utilized for the computations. The computations were performed using a time-step of 10^{-2} seconds. The convergence criteria was to reduce the residuals of all equations to 10^{-4} at each time step.

DESIGN OPTIMIZATION

The first step in the computation algorithm was to assume a total number (N) of TES modules. Assuming N>1, the total number of TES modules can be simulated to operate either in series or in parallel configuration. The configuration is important because it will dictate the form in which boundary conditions will be specified. The second step was to calculate the thermal power added to each TES module by dividing the total storage capacity of the TES system by the total number of TES modules (kW/module). The third step was to estimate the volumetric heat generation in the electrical heaters (W/m^3) by dividing the thermal power added to each TES module by the total circular fin volume (m^3). As previously stated, the volumetric heat generation is specified across all circular fins. The fourth step was to determine the total hours of charge time and discharge time. Table 1 summarizes the parameters chosen for the computations.

Having determined the system's charge computation parameters, a transient computation solving for energy equations only was set up for the specified number of charge hours. Joule heating was specified at the fins in the form of volumetric heat generation. Because the charge computation simulated the heat transfer from the fins to the concrete through conduction, flow equations were not solved. At this stage, heat was generated in the fins and transferred to the concrete body via thermal conduction. Once the charge computation completed and the end-of-charge temperature values were saved for each major component, a steady-state flow computation was started using the k-ε turbulence model with standard wall functions. At this stage, the energy equation was disabled and flow equations enabled. The purpose of the flow computation step was to converge the flow before initiating the discharge computation. This is critical in order to reduce the total amount of computation time at the discharge stage. When the convergence of the flow field computations was achieved, a transient discharge computation solving for the energy equation was set up to simulate the transfer of thermal energy from the concrete to the air passing through the tubes.

Table 1 – Input Conditions

Thermal Power Added per Module (kW)	**50**
Volumetric Heat Generation (kW/m3)	**782,602**
Charge Time (hours)	**6**
Discharge Time (hours)	**6**
Mass Flow Rate per Tube (kg/s)	**0.25**
Inlet Temperature (K)	**600**

The final step in the calculation algorithm was to evaluate the temperature of air at the outlet of the HTES. This can be done by inspecting the air exit temperature profile. If the air exit temperature is not within the acceptable range (> 850 K), the next TES module in series was needed to improve the exit air temperature profile. All steps were repeated for the following TES modules with the exception of the inlet boundary condition at the discharge cycle. At this stage, the transient exit air temperature profile leaving the previous TES module is specified as a boundary condition at the inlet of the next TES module. The process is repeated until conditions have been met up to the total number of N modules initially selected.

RESULTS AND DISCUSSION

The heat transfer from the storage medium (concrete) to the air in the HTES is investigated during the discharge cycle. The results indicate that 12 TES modules are required to provide the expander in Fig. 1 with 6 hours of air temperature above 850 K. Figures 5-6 illustrate the average temperatures of major components of the HTES during the entire charge-discharge cycle for the first and last TES modules (TES Module 12). The charge cycle begins from 0 to 6 hours and the discharge cycle begins from 6 hours to 12 hours. Because thermal losses are ignored in this study and the heat is generated within the HTES, a linear function of the average temperatures is expected versus time during charging. This behavior can be seen in Figs. 8-9, from 0 to 6 hours. Of special importance is the exit air temperature profile, which can be seen during the discharge cycle from 6 hours to 12 hours. As noted previously, an important aspect of the TES design is to deliver air temperature above 850 K for over 6 hours. As shown in Fig. 8, the air exit temperature of the first TES module falls below the desired temperature in about 15 minutes; therefore, it was necessary to consider additional TES modules in series to raise the exit air temperature. Twelve TES modules in series were found to deliver an average exit air temperature of 850 K over 6 hours.

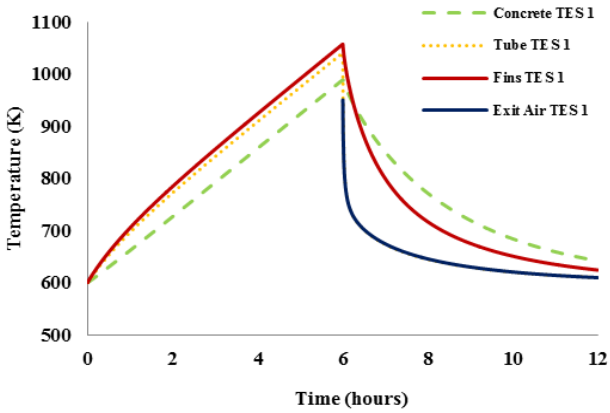

Figure 5 – Average Temperatures (K) at End of Discharge Cycle for TES Module 1.

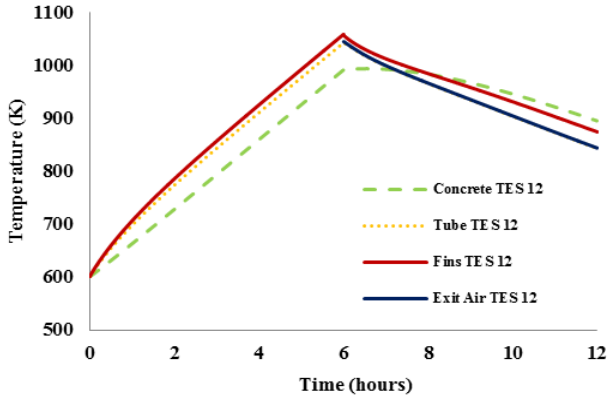

Figure 6 – Average Temperatures (K) at End of Discharge Cycle for TES Module 12.

Figure 7 shows the temperature contours of the concrete at the end of the discharge cycle of the last TES module. At this phase, a majority of the energy stored in the concrete has been extracted by the air passing through the air tubes. The areas of higher temperature, denoted by the red color, are the corners of the concrete body furthest from the center tubes. The total amount of energy added to the TES module can be estimated by the following equation:

$$Q_A = M_C(c_p)_C \Delta T_C + M_F(c_p)_F \Delta T_F + M_T(c_p)_T \Delta T_T \quad (8)$$

where Q_A is the thermal energy generated in the HTES during the charge cycle through Joule heating. Similarly, the total amount of energy extracted from the TES can be estimated by the following equation:

$$Q_E = M_C(c_p)_C \Delta T_C + M_F(c_p)_F \Delta T_F + M_T(c_p)_T \Delta T_T \quad (9)$$

where Q_E is the energy extracted by the TES during the discharge cycle. All variables remain the same, with the exception of ΔT, which now becomes the average temperature difference between the temperature at the end of the charge cycle and the temperature at the end of the discharge cycle.

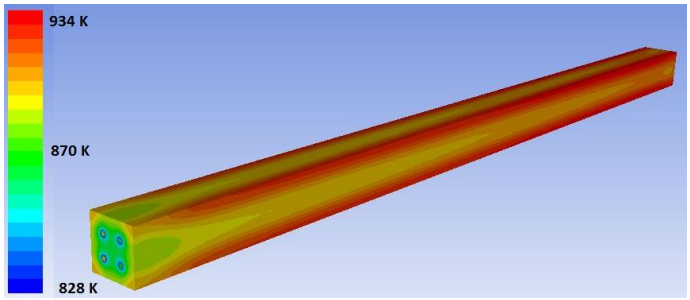

Figure 7 – Temperature contour plot at the end of discharge cycle for last TES module (TES 12).

Equation (8) estimates the percentage of energy that is added to the HTES during charging and Eq. (9) finds the amount of thermal energy that is extracted and provided to the air flow. The theoretical amount of energy added to the system (kWh) is the total capacity of the system (kW) times the number of charge hours. Thus, the efficiency of the system in transferring energy to the TES can be determined by formulating a ratio of Eq. (8) to the theoretical amount of energy added to the system, where ratios close to 1 indicate that the system transferred a majority of the heat from the resistance heaters to the concrete.

Figure 8 shows the average exit air temperature of all twelve TES modules in series. This figure reveals that a system of cascaded TES modules will gradually increase the exit air temperature by an average of 20 K at every TES module. The total number of TES modules in series is determined by the average exit air temperature that is required at the expander. Figure 9 illustrates the temperature of the concrete after the end of 6 hours of discharge. The results show that a majority of the

energy extracted from the concrete body by the air occurs at the initial stages of the cascaded TES system. By the time the air flow reaches the final stages of the cascaded system, the energy extraction is minimal. The remaining thermal energy in the HTES contributes to priming the system for the next cycle, in which thermal generation in the HTES should be controlled in each module independently.

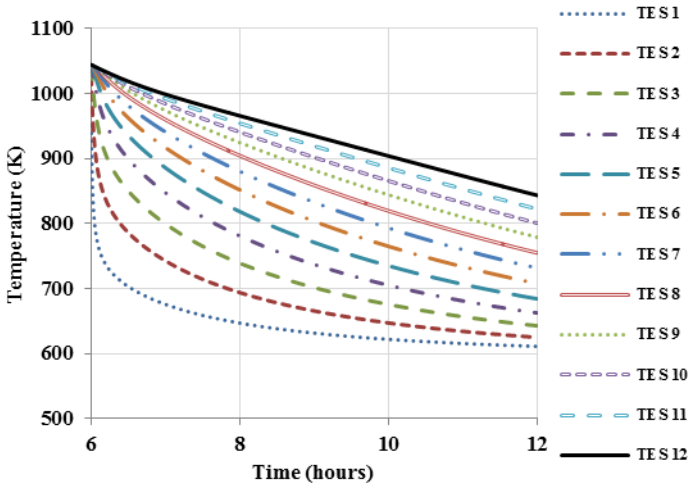

Figure 8 – Air exit temperature of all 12 modules during discharge cycle.

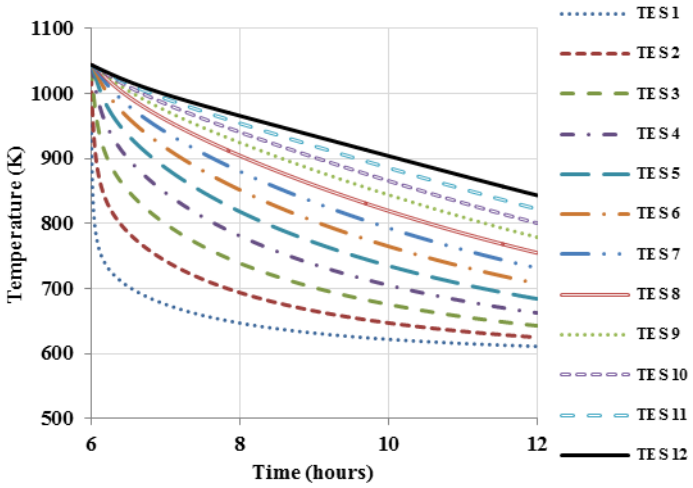

Figure 9 – Average temperature of solid-state storage medium during discharging for all 12 modules.

In addition to better control of resistance heating, ongoing work is being conducted to determine how the TES system can more effectively meet changes in grid demand. It is important to note that any mass flow turndown or adjustments to resistance heating has a direct impact on the round trip efficiency, total system efficiency, and the total exhaust power that can be delivered by the microturbine in the HTH-CAES system. Therefore, special attention must be devoted when adjusting any of these two critical parameters.

CONCLUDING REMARKS

In this study, a modular solid-state TES system was designed and investigated computationally. It was shown that a concrete-based TES incorporating an array of circular fins with embedded heaters can be used to store the energy of the grid in the form of heat. The computations of this study reveal that 12 modules of the designed TES system will provide the high temperature hybrid compressed air energy storage with 6 hours of air flow at 850 K.

The temperature distribution at the end of the discharge shows that significant amount of thermal energy remains in the HTES after discharge and should be utilized for priming the HTES. The thermal energy residues in the HTES require the next charge cycles to be performed in a controlled manner to prevent excessive temperatures from the electric heaters.

The focus of future work for this effort is on developing a refined design that can satisfy dynamic changes in peak demand and meet the system's performance requirements. This task requires further computational and experimental studies on different configurations of geometry to determine a design that is cost-efficient.

ACKNOWLEDGMENT

This study was supported by award No. EPC-14-027 granted by California Energy Commission (CEC), and California State Polytechnic University Pomona's Research, Scholarship, and Creative Activities (RSCA) award.

NOMENCLATURE

C_μ, $C_{1\varepsilon}$, $C_{2\varepsilon}$, $C_{3\varepsilon}$	Empirical constant of k-ε model
$(C_p)_C$	Specific heat of concrete (J/kg.K)
$(C_p)_F$	Specific heat of fins (J/kg.K)
$(C_p)_T$	Specific heat of tubes (J/kg.K)
g = 9.81	Gravity (m/s^2)
G	Energy generation due to joule heating (W/m^3)
G_b	Turbulence generation due to buoyancy (N/m.s^2)
G_k	Turbulence generation due to shear (N/m.s^2)
h	Sensible enthalpy (J/kg)
i,j	Dummy variables
k	Turbulent kinetic energy (N.m.s^2)
M_C	Total mass of concrete (kg)
M_F	Total mass of fins (kg)
M_T	Total mass of tubes (kg)
Q_A	Energy added to TES (kWh)
Q_E	Energy extracted from TES (kWh)
Q_{in}	Energy added to HTES (kWh)
S_{ij}	Strain Rate Tensor (m/s)
ΔT_C	Temperature delta of concrete (K)
ΔT_F	Temperature delta of fins (K)
ΔT_T	Temperature delta of tubes (K)
v_j	Velocity components (m/s)
x_j	Spatial coordinates (m)

Greek symbols

ε	Dissipation rate of turbulent energy (N/m.s^2)
$\sigma_\varepsilon, \sigma_k$	Empirical constants of k-ε model
σt	Turbulence Prandtl number
ϱ	Density of storage fluid (kg/m^3)
λ	Thermal conductivity of SF (W/m.K)
$\lambda_t = \frac{c_p \mu_t}{\sigma_t}$	Eddy thermal conductivity (W/m.K)
μ	Viscosity of storage fluid (Pa-s)
μ_t	Eddy Viscosity (Pa-s)

REFERENCES

[1] Toward a 21st Century Electricity System in California, 2015, Advanced Energy Economy Institute (AEEI).

[2] F. Crotogino, K-U. Mohmeyer, and R. Scharf. Huntorf, 2001, CAES: More than 20 years of successful operation. In SMRI Spring Meeting.

[3] Ter-Gazarian, 1994, A. Energy Storage for Power Systems. Stevenage, Harts., U.K.: P. Peregrinus on Behalf of the Institution of Electrical Engineers.

[4] RWE Power, 2010, ADELE – Adiabatic Compressed Air Energy Storage for Electricity Supply. RWE Power AG, Essen/Koln.

[5] Houssainy, S, Lakeh, R.B., Kavehpour, H.P., 2016, A Thermodynamic Model of A High Temperature Hybrid Compressed Air Energy Storage System for Grid Storage, Paper No. PowerEnergy2016-59431, Proc. of the ASME 2016 Power and Energy Conference, Charlotte, NC.

[6] Baghaei Lakeh R., Lavine, A.S., Kavehpour H.P., Ganapathi G. B., Wirz, R. E., 2013, "The Effect of Laminar and Turbulent Natural Convection on Supercritical Thermal Storage," Numerical Heat Transfer – Part A, vol. 64, pp. 955-973.

[7] Baghaei Lakeh R., Lavine, A.S., Kavehpour H. P., Ganapathi G. B., Wirz, R. E., 2013, "Effect of Natural Convection on Thermal Energy Storage using Supercritical Fluids," Paper No. ESFuelCell2013-18079, Proc. of 7th ASME Int. Conference on Energy Sustainability Minneapolis, MN.

[8] Baghaei Lakeh R., Kavehpour H.P., Lavine, A.S., Ganapathi G. B., Wirz, R.E., 2013, "Study of Turbulent Natural Convection in Vertical Storage Tubes for Supercritical Thermal Storage System," Paper No. IMECE2013-62716, Proc. of the ASME International Mechanical Engineering Congress and Exposition, San Diego, CA.

[9] Baghaei Lakeh R., Lavine, A.S., Kavehpour H.P., Wirz, R. E., 2015, "Study of Turbulent Natural Convection in Vertical Storage Tubes for Supercritical Thermal Energy Storage," Numerical Heat Transfer – Part A, vol. 67, pp. 119-135.

[10] Dincer, I., Rosen, M.A., 2010, "Thermal Energy Storage: Systems and Applications," 2nd Ed., John Wiley & Sons, Chichester, UK.

[11] Launder, B.E., Spalding, D.B., 1974, "The Numerical Computation of Turbulent Flows," Computer methods in applied mechanics and engineering, 3, pp. 269-289.

[12] Launder, B.E., Spalding, D.B., 1972, "Lectures in Mathematical models of turbulence," 1st ed., Academic Press, London, UK.